Simulated Interactions between Angiotensin-Converting Enzyme and Substrate Gonadotropin-Releasing Hormone: Novel Insights into Domain Selectivity†

Athanasios Papakyriakou,‡ Georgios A. Spyroulias,*,‡ Edward D. Sturrock,|| Evy Manessi-Zoupa,§ and Paul Cordopatis‡

Departments of Pharmacy and Chemistry, University of Patras, Panepistimioupoli−Rion, GR-26504, Greece, and Division of Medical Biochemistry, Institute of Infectious Disease and Molecular Medicine, University of Cape Town, Rondebosch 7701, South Africa

Received February 6, 2007; Revised Manuscript Received May 2, 2007

ABSTRACT: Human angiotensin-I converting enzyme (ACE) is a central component of the renin-angiotensin system and a major target for cardiovascular therapies. The somatic form of the enzyme (sACE) comprises two homologous metallopeptidase domains (N and C), each bearing a zinc active site with similar but distinct substrate and inhibitor specificities. On the basis of the recently determined crystal structures of both ACE domains, we have studied their complexes with gonadotropin-releasing hormone (GnRH), which is cleaved releasing both the protected NH_2- and COOH-terminal tripeptides. This is the first molecular modeling study of an ACE−peptide substrate complex that examines the structural basis of ACE's endopeptidase activity and offers novel insights into subsites that are distant from the obligatory binding site and were not identified in the crystal structures. Our data indicate that a bridging interaction between Arg500 of the N-domain and Arg^8 of GnRH that involves a buried chloride ion may account for its role in the specificity of the N-domain for endoproteolytic cleavage of the substrate at the NH_2-terminus *in vitro*. In support of this, the protected NH_2-terminal dipeptide of GnRH exhibits stronger interactions than the protected COOH-terminal dipeptide with the N-domain of ACE. Further comparison of the models of ACE−substrate complexes promotes our understanding of how the two domains differ in their function and specificity and provides an extension of the pharmacophore model used for structure-based drug design up to the S_7 subsite of the enzyme.

Hypertension is a major risk factor in cardiovascular and kidney disease, affecting a quarter of the world's adult population (*1*). The development of novel therapeutic approaches has focused on the renin−angiotensin system (RAS), which plays a key role in the regulation of blood pressure and electrolyte balance in humans (*2*). In the main pathway of the RAS, renin acts on the circulating precursor angiotensinogen to generate the decapeptide angiotensin (Ang) I, which is converted by angiotensin-I converting enzyme (ACE[1]) to the potent vasopressor octapeptide Ang II. In parallel, ACE affects blood pressure by inactivating bradykinin (BK) and kallidin, vasodilator peptides which are generated from kininogen by the action of kallikrein (*3*). Because of this dual function, ACE inhibitors have been first line antihypertensive therapies for many years (*4*−*7*).

ACE (EC 3.4.15.1) is classified as a member of the M2 gluzincin family within the MA clan (*8*, *9*). There are two isoforms of ACE that are transcribed from the same gene in a tissue-specific manner (*10*): the somatic form (sACE) that is found in a variety of tissues and the testicular form (tACE), which is exclusively expressed in germinal cells. sACE is a 1,277-residue type I transmembrane glycoprotein with an ectodomain consisting of two highly homologous parts (N and C domains). tACE is a 701-amino-acid isoform that except for the first 36 residues is identical to the C domain of sACE (*11*). Each domain contains an active site bearing the characteristic HEXXH zinc-binding motif of Zn-peptidases (zincins) (*12*). The sequence and structural homology at the active sites of ACE favors an enzymatic mechanism analogous to that proposed for thermolysin (*13*). This hydrolytic reaction proceeds via a general-base mechanism with the nucleophilic attack of a water molecule or hydroxide ion on the carbonyl carbon of the scissile bond (*14*).

The recent breakthrough in determining the high-resolution crystal structures of human tACE (C domain of sACE) (*15*) and that of the N domain of sACE (*16*), both in the absence and presence of the potent inhibitor lisinopril, has renewed the interest in the study of their enzymatic activity at a molecular level and has provided a structural basis for the design of domain-specific inhibitors (*17*, *18*). Despite the structural homology of the two domains of sACE, which have ∼60% sequence identity, some notable differences between the active sites were observed (*16*). Consistent with the observed chloride-dependent activation of ACE (*19*), only

† A.P. has been supported by a postdoctoral scholarship from the Greek National Foundation of Scholarships (IKY).

* To whom correspondence should be addressed. Tel: +30 2610969950 and -951. Fax: +30 2610969950. E-mail: G.A.Spyroulias@upatras.gr.

‡ Department of Pharmacy, University of Patras.

§ Department of Chemistry, University of Patras.

|| University of Cape Town.

[1] Abbreviations: ACE, angiotensin-I converting enzyme; sACE, somatic ACE; tACE, testis ACE; nACE: N-domain of sACE; cACE: C-domain of sACE; GnRH: gonadotropin-releasing hormone; Ang: angiotensin, BK: bradykinin; rmsd: root-mean-square deviation.

10.1021/bi700253q CCC: $37.00
Published on Web 07/03/2007

Table 1: Sequences of the Natural Substrates Ang I, Ang_{1-7}, BK, and GnRH in Two Orientations for C-Terminal ($GnRH_C$) and N-Terminal Endopeptidase Cleavage ($GnRH_N$)[a]

P_8	P_7	P_6	P_5	P_4	P_3	P_2	P_1	P_1'	P_2'	P_3'	
Asp	Arg	Val	Tyr	Ile	His	Pro	Phe^8	His^9	Leu		Ang I
			Asp	Arg	Val	Tyr	Ile^5	His^6	Pro		Ang_{1-7}
	Arg	Pro	Pro	Gly	Phe	Ser	Pro^7	Phe^8	Arg		BK
	pGlu	His	Trp	Ser	Tyr	Gly	Leu^7	Arg^8	Pro	nGly	$GnRH_C$
	nGly	Pro	Arg	Leu	Gly	Tyr	Ser^4	Trp^3	His	pGlu	$GnRH_N$

[a]pGlu is the N-terminus pyroglutamic acid, and nGly is the amidated C-terminus Gly residue of GnRH.

one chloride ion was bound to the N domain as opposed to the two found in the crystal structure of tACE (*16*). In addition, tACE has been co-crystallized with the antihypertensive drugs captopril and enalaprilat (*20*).

The most common small-molecule inhibitors exhibit comparable selectivity for both active sites (*21*), whereas the N domain is 1000-times more sensitive to inhibition by the phosphinic peptide RXP407 (*22*) and more than 3000-times less sensitive to inhibition by RXPA380 (*23*). Both domains hydrolyze the principal physiological peptides Ang I and BK at comparable rates but with different chloride concentration requirements (*24*). Whereas the enzymatic activity of the C domain is highly dependent on chloride concentration, that of the N domain is much less so (*24*).

Interestingly, ACE exhibits endopeptidase activity for substrates with amidated C-termini such as substance P and gonadotropin-releasing hormone (GnRH, formerly known as luteinizing hormone-releasing hormone or LHRH) by cleaving their C-terminal tripeptides. Other natural substrates with high specificity for the N domain are Ang_{1-7} (*25*) and N-acetyl-SDKP, the latter being involved in the control of the hematopoietic stem cell proliferation (*26*). Because of its protected amino-terminal pyroglutamic acid, GnRH is also metabolized to release the N-terminal tripeptide, in addition to the C-terminal tripeptide (Table 1) (*27*). The N domain of ACE is mainly responsible for the primary amino-terminal endoproteolytic cleavage of GnRH, whereas carboxy-terminal cleavage is performed by both active sites of ACE *in vitro* (*24*, *28*).

The unique endopeptidase activity of ACE for GnRH, in conjunction with the available crystal structures of both enzymatic domains, has motivated our *in silico* studies of their complexes. With the aim of gaining structural information regarding the interaction of the enzyme−substrate complexes, GnRH was docked into the catalytic channel of both ACE domains, in the appropriate orientation for either COOH- or NH_2-terminal cleavage. Molecular dynamics calculations have been employed as a means to allow for enzyme reorganization in the presence of substrate. All simulations were carried out with explicit solvent representation so as to examine the effect of solvent molecules in mediating intermolecular interactions. This study extends our knowledge of the structural determinants that contribute to substrate specificity, which will aid the design of second-generation domain-specific ACE inhibitors.

COMPUTATIONAL METHODS

Structure Preparation. The crystal structure coordinates of ACE−lisinopril complexes were obtained from RSC: pdb code 1O86, for the C domain (tACE) and pdb code 2C6N, for the N domain of sACE. All heteroatoms with the exception of zinc and chloride ions were removed. Missing atoms and hydrogen atoms were added using the LEaP module of AMBER 8 (*29*). The protonation state of ionizable groups was predicted by the program H++ using a continuum electrostatic model with the Poisson−Boltzmann method (*30*). In addition to this, visual inspection of all histidine residues for hydrogen bonding ability with their neighboring residues was performed. The added atoms were subjected to 500 rounds of energy minimization with steepest descent gradients, while all other atoms were kept fixed by applying 50 $kcal \cdot mol^{-1} \cdot Å^{-2}$ positional restraints. Implicit solvent was applied using the generalized Born model GB^{HCT} (*31*) with 16 Å cutoff for the nonbonded interactions. GnRH structure was also generated using LEaP and was subjected to energy minimization in implicit solvent. For the pyroglutamic acid residue, GAFF parameters (*32*) and AM1-BCC partial atomic charges (*33*) were assigned by the AMBER module Antechamber. His^2 residue of GnRH was assigned its protonated form.

Docking of the Substrates. The program AutoDock 3.05 (*34*) was used for all docking calculations, and AutoDockTools was used for visual inspection of the docking results. Protein and ligands were treated with the united-atom approximation by merging all nonpolar hydrogens. Kollman partial charges were assigned to all protein atoms, whereas for zinc and chloride ions, formal charges and van der Waals parameters from the AMBER database were assigned. The Lamarckian genetic algorithm was employed with the following standard parameters: a population size of 50 individuals; a maximum number of 1.5×10^6 energy evaluations and a maximum number of 27,000 generations; an elitism value of 1; a mutation rate of 0.02; and a crossover rate of 0.80 (*34*). For most of the calculations, 100 docking rounds were performed with step sizes of 0.25 Å for translations and 5° for orientations and torsions. Docked conformations were clustered with 1.5 Å tolerance for the root-mean-square positional deviation.

Because of the relatively high conformational freedom of the decapeptide substrate, its docking into the catalytic channel of ACE with the scissile bond in the appropriate orientation is practically difficult. For this reason, we have performed the docking of $GnRH_{1-5}$ and $GnRH_{6-10}$ in two steps, and their docked conformations were then linked together. Two grid maps for each domain of ACE, one centered at the S_2-S_1-S_1'-S_2'-S_3' subsites (zinc-binding site) and the other at the S_7-S_6-S_5-S_4-S_3 subsites (substrate channel), were calculated using AutoGrid with $81 \times 81 \times 81$ grid points of 0.25 Å spacing. The two grid maps overlapped at the S_3-S_2 subsite. In order to acquire the $GnRH_C$ conformation, $GnRH_{1-5}$ was docked into the substrate channel and $GnRH_{6-10}$ at the zinc binding site and vice versa for $GnRH_N$. Selection of the conformations from the docking calculations is based on different criteria for each part of the substrate. When referring to the accepted conformations at the ACE zinc-binding domain, two criteria should be satisfied: (I) the distance between Leu^7 ($GnRH_C$) or Trp^3 ($GnRH_N$) carbonyl oxygen and zinc is shorter than 3.0 Å, and (II) the N-terminus of Gly^6 ($GnRH_C$) or the C-terminus of Tyr^5 ($GnRH_N$) is oriented toward the substrate channel domain. For the substrate channel domain, a docked conformation is accepted when the distance between the

C-terminus carbon of Tyr^5 and the N-terminus nitrogen of Gly^6 is shorter than 4.0 Å.

However, the choice of an appropriate conformation for each fragment is hampered by the extensive conformational space of the pentapeptides. For instance, even after 100 rounds of docking Gly^6−$nGly^{10}$ into the zinc-binding domain of nACE, there was no acceptable solution. The docked conformations that fulfilled criterion I did not have the expected orientation of the N-terminal group, whereas those consistent with criterion II were at an inappropriate distance from the zinc. Therefore, performing 200−300 rounds of docking was necessary. In order to achieve an increased number of conformations that fulfill criteria I and II, the charge of Leu^7O was changed from −0.50 to −1.50 e. In this way, at least two accepted conformations of the Gly^6−$nGly^{10}$ fragment at the zinc-binding domain of nACE were obtained per 100 docking rounds. Docked conformations were ranked by the predicted binding energy, though the final choice was also based on visual inspection of the enzyme−substrate interactions, in order to verify that accommodation of the P_2-P_1-P_1' side chains is reasonable according to the X-ray crystal structures of both ACE domains with lisinopril (see Results and Discussion).

After having selected the appropriate P_2−P_3' conformation, P_2 and P_1 moieties were included in the calculation of the second grid, being regarded as part of the substrate channel. Consequently, each predicted conformation of the P_7−P_3 fragment occupied distinct sites from those of the zinc-binding domain fragment so that all accepted conformations were productive. The top-ranked binding modes among the accepted conformations were also visually inspected in order to validate that intermolecular interactions were predicted properly; in particular, whether H-bonding donor and acceptor atoms were correctly positioned and whether hydrophobic residues lay inside hydrophobic subsites of the enzyme. In this fashion, the choice of the P_7−P_3 fragment depends on both the value of the predicted binding energy as well as its reasonable placement inside ACE, with the latter influenced by the presence of the zinc-bound GnRH moiety (see Results and Discussion). Subsequently, $GnRH_{1-5}$ and $GnRH_{6-10}$ were linked together, and a bond between the oxygen of the scissile bond and zinc was created using LEaP. At this point, a TIP3P water molecule was placed between the scissile bond and Glu411/389 (cACE/nACE), which was also linked to zinc. Each ACE−substrate complex was subjected to energy minimization as described above while constraining the movement of all enzyme atoms. Torsional angle restraints were imposed when necessary to keep the Tyr^5−Gly^6 peptidic bond of GnRH in the trans-conformation.

Molecular Dynamics. All calculations were carried out using SANDER and PMEMD programs of AMBER 8 (*29*). The force field of Cornell et al. (*35*) was employed with full representation of solvent using the TIP3P water model (*36*). Periodic boundary conditions were imposed by means of the particle mesh Ewald method with an 8 Å limit for the direct space sum. Numerical integration was performed with a 2-fs time step, and all bonds involving hydrogen atoms were constrained with SHAKE (*37*). Temperature and pressure controls were imposed using a Berendsen-type algorithm (*38*) with coupling constants of 1.0 and 5.0 ps, respectively. Force field parameters for the zinc-binding sites have been added as described below. The protein−substrate complexes were immersed in isometric truncated octahedron water boxes, constructed from a cubic box of ∼90 Å, and an appropriate number of Na^+ ions was added to neutralize the system. The following procedure was used in order to equilibrate the position of solvent molecules, the temperature, and the pressure of the system: (a) energy minimization for 100 steps with steepest descent and 900 steps with conjugate gradients was performed by imposing 50 kcal·mol^{-1}·Å^{-2} positional restraints on the solute atoms; (b) temperature was gradually increased at 300 K (in 50 K steps) within six rounds of 5-ps constant volume dynamics, while solute atoms were kept fixed by imposing 10 kcal·mol^{-1}·Å^{-2} restraints; (c) restraints were then released within 20 ps in the NVT at 300 K; and (d) the density of the simulation box was increased from 0.90 to 1.05 g·cm^{-3} within 150 ps of constant pressure dynamics. Subsequently, production runs of 2,000−3,000 ps were carried out at physiological conditions (300 K, 1 atm) in the NPT ensemble. The translational center-of-mass motion was removed every 1000 steps, and trajectories were updated every 500 steps (viz. every ps). For visual inspection and analysis of the MD trajectories, the program VMD 1.8 (*39*) was used. Solvent-accessible and buried surface areas were calculated by the program MSMS 2.5 (*40*) with a probe radius of 1.5 Å within VMD. The Figures were also prepared with VMD and plots using the program GRACE 5.1.

Zinc Force Field Parameters. The zinc coordination sphere in native ACE comprises His383/361, His387/365, Glu411/389 (C-/N-domain numbering), and a solvent molecule. In accordance with a well-accepted proposal for thermolysin (*13*, *14*), ACE−substrate complexes involve an analogous pentacoordinated metal center. As soon as the substrates are positioned in the central channel of the enzyme, the carbonyl oxygen of the scissile bond binds to zinc by displacing the zinc-bound water toward Glu384/362. We initially experimented with a nonbonded metal representation, using the parameters proposed by Stote and Karplus (*41*). However, we found that during the equilibration period, water moved toward the P_2 side of the substrate. Consequently, Glu384/362 came to within a distance of 2.0 Å from zinc and remained there for the rest of the simulation (data not shown). Such a tendency of zinc to be hexacoordinated during unrestrained MD calculations has been also observed by others using the nonbonded approach with the AMBER force field (*42*, *43*).

For this reason, we adopted the bonded approach with explicit bonds between the metal and its ligands. Force field parameters were derived from hybrid B3LYP density functional calculations using GAUSSIAN 98 (*44*). A model of the active site (Figure 1 in Supporting Information), was extracted from the high-resolution crystal structure of tACE. The inhibitor was replaced by a water molecule opposite Glu411, and *N*-methylacetamide was docked as the substrate. The HEMGH...E zinc-binding motif was retained, except that Met was truncated into Gly and Glu411 into butyrate. Geometry optimizations were then carried out with loose convergence criteria using the LANL2DZ basis, which was shown to perform quite well for analogous systems (*45*). For comparison, 3-21G*/ and 6-31G*/B3LYP geometry optimizations were also carried out. Analogous force fields by others (*46*, *47*) were taken into consideration in extracting

the bond and angle parameters shown in Table 1 of the Supporting Information. All dihedral angle parameters including zinc were set to zero. The partial atomic charge of zinc was set to +0.75 e, and the standard AMBER charge of the five ligand atoms was increased by +0.25 e (i.e., the two histidine $N_\epsilon 2$, the glutamate $O_\epsilon 1$, the zinc-bound water oxygen, and the carbonyl oxygen of the substrate). This minimal charge distribution is in good agreement with partial charges reported for zinc and its coordinating atoms (*48*, *49*) by using the RESP fit method (*50*). The same Lennard−Jones parameters as for the docking calculations ($R^* = 1.10$ Å, $\epsilon^* = 0.0125$ kcal·mol^{-1}) were employed (*46*).

The additional set of AMBER force field parameters (Table 1 in Supporting Information) was assessed during the course of molecular dynamics simulations by examining the geometry of the zinc coordination sphere of the ACE−GnRH complex in both orientations. The plots of zinc−ligand bond and angle values as a function of simulation time (Figures 2 and 3 in Supporting Information) exhibit a well-defined geometry that is in agreement with that provided by the B3LYP density functional calculations. A minor point is that Zn−OW and Zn−N of histidine exhibit shorter bonds in comparison with those extracted from DFT calculations by ~0.2 and ~0.1 Å, respectively. As far as the imidazole N8/N9−Zn−O angles are concerned, depending on the system under study they exhibit a fluctuation between 110° and 140°. This observation is in accordance with our DFT calculations when comparing results from different basis sets, which led us to assign the same value for both angle parameters (i.e., $\theta_o = 125°$).

RESULTS AND DISCUSSION

For the sake of simplicity in making direct comparisons between the two opposite orientations of GnRH in the S primed and non-primed subsites of both ACE domains, residues of $GnRH_N$ toward the N-terminus are numbered $P_1'-P_3'$, and those toward the C-terminus are numbered P_1-P_7, as shown in Table 1. For the same reason, tACE that corresponds to the C domain of sACE is referred as cACE and to the N domain of sACE as nACE.

Docking of the Substrate. Prediction of small molecule or short peptide binding modes becomes quite straightforward because of the available crystal structures of ACE with the bound inhibitor lisinopril (*15*, *16*). The binding subsites S_1, S_1', and S_2' are well characterized, and the differences at the active sites between the two domains of ACE are documented (*16*). However, obtaining models of ACE with larger substrates, such as GnRH, introduces two major difficulties: first, subsites S_7-S_2 and S_3' need to be identified, and second, a decapeptide such as GnRH occupies a relatively large conformational space inside the catalytic groove of ACE. In conjunction with the enzyme's plasticity and reorganization upon binding of the substrate, prediction of the interactions that dominate their complex is a challenging task. To overcome this, we have carried out a fragment- and knowledge-based docking method followed by molecular dynamics calculations. In the first stage of this approach, a binding conformation of the substrate is obtained by flexible docking of two peptidic fragments: one that brackets the scissile bond, of which the carbonyl oxygen binds zinc, and one for the remaining residues. In the case of GnRH, the two fragments comprise $pGlu^1-Tyr^5$ and Gly^6-nGly^{10} (Table 1). Each fragment is docked at two overlapping binding sites, one centered at the zinc-binding domain and the other centered at the central groove and parallel to helices α1 and α2. In order to obtain the proper GnRH orientation for carboxy terminal cleavage ($GnRH_C$), the Gly^6-nGly^{10} fragment is docked at the zinc-binding site and $pGlu^1-Tyr^5$ at the substrate channel. In the opposite orientation for amino terminal cleavage ($GnRH_N$), docking is performed with Gly^6-nGly^{10} at the substrate channel and $pGlu^1-Tyr^5$ at the zinc-binding domain (Figure 1).

Even for the pentapeptide fragments of GnRH with 18 and 15 flexible torsions for $pGlu^1-Tyr^5$ and Gly^6-nGly^{10}, respectively, the conformational space is still large enough to be sampled adequately. The possibility of applying distance restraints between ACE and GnRH during the docking procedure would have significantly increased the number of accepted conformations. Given that distance restraints between a ligand and a protein atom cannot be imposed using AutoDock, the negative charge of the Leu^7 carbonyl oxygen was increased, so as to achieve an increased number of docked conformations with the appropriate orientation of the scissile bond. It should be noted that the increase of the negative charge of the ligand results in overestimation of the calculated binding energies because of the artificially increased electrostatic energy of the Zn···O pair. This approach is only suitable to compensate for a weak distance restraint between the two opposite charges. Indeed, the number of accepted conformations of $GnRH_C$ at the zinc-binding domain of cACE is increased significantly upon changing the charge of Leu^7O as well as the estimated energies that are higher by ~3 kcal·mol^{-1} (Table 2). At this point, the accepted conformations were evaluated by comparing the binding mode of P_1-P_2' with that of the crystallographic position of the inhibitor complexes. In this way, use of the experimental data on the distinct S_1-S_2' subsites of ACE render the choice of the structure to be used for subsequent MD calculations simpler. Thus, the highest affinity conformation that exhibits a reasonable binding mode with respect to the cocrystalized inhibitor was chosen (Figure 2).

As far as the second $GnRH_C$ fragment is concerned, docking of $pGlu^1-Tyr^5$ into the substrate channel of cACE produced 12 accepted conformations per 100 docking rounds (Table 2). However, nine of these exhibited major steric hindrances with the Gly^6-nGly^{10} fragment, which was also the case for nACE for both GnRH orientations. For this reason, after having selected the top-ranked conformation of the zinc-bound fragment, residues P_2-P_1 were included in the substrate channel grid box for the subsequent docking calculations. Using this approach, all solutions for the P_7-P_3 fragment are prevented from overlapping with the selected P_2-P_1 moiety of the zinc-binding domain, as illustrated in Figure 4 of the Supporting Information for the corresponding $GnRH_C$ fragments. The calculated binding energies are higher than those calculated in the absence of the P_2-P_1 fragment by ~1.0 kcal·mol^{-1} (Table 2), a result that is attributed to the increased electrostatic contribution of the $P_3\cdots P_2$ charged termini. A similar approach has been applied by McCammon and co-workers in the relaxed-complex scheme that permits the design of potent drugs by combining two or three ligand fragments with weak affinity (*51*). The higher affinity ligand

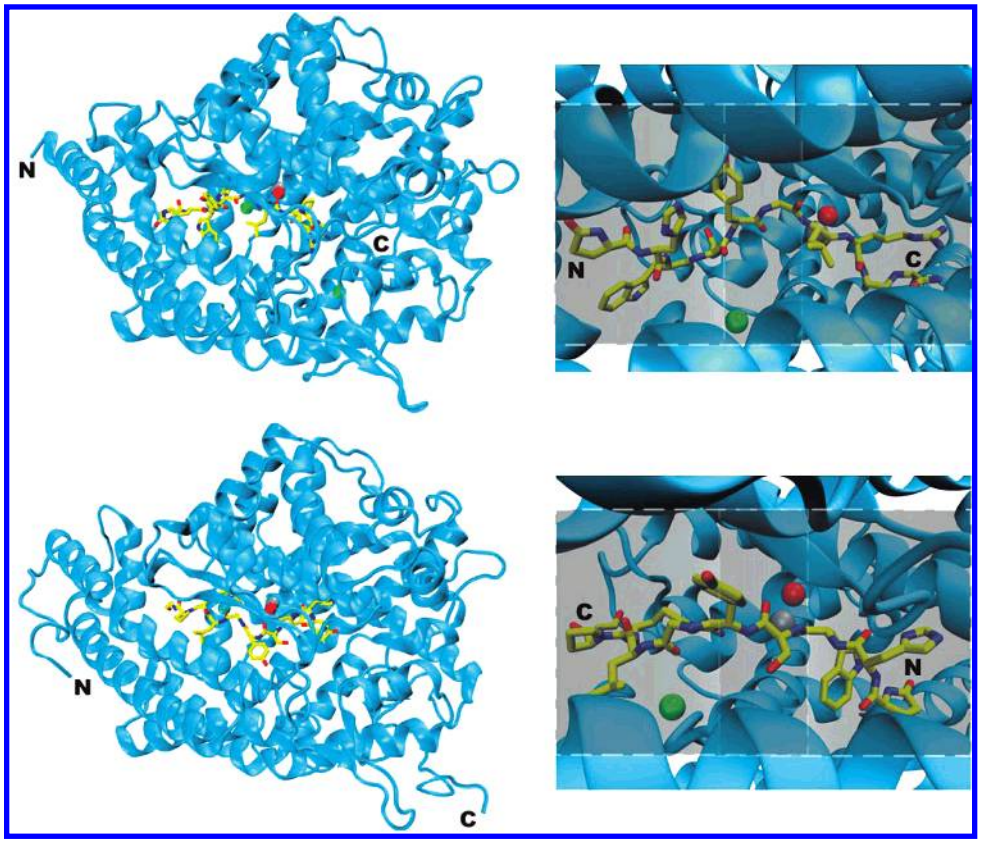

FIGURE 1: Cartoon of ACE C-domain (and cACE, upper panel) and N-domain (nACE, lower panel) with GnRH shown as yellow sticks, zinc as gray, the zinc-bound water as red, and the buried chloride ions as green spheres. GnRH is shown either docked for carboxy terminal cleavage ($GnRH_C$, upper) or for amino terminal cleavage ($GnRH_N$, lower).

Table 2: Comparison of the Results Obtained for $GnRH_C$ Docking to cACE between Two Approaches for Each of the Substrate Parts[a]

GnRH fragment	ACE domain	no. of accepted conformations	mean docked energy	mean binding energy	mean rmsd
A. Gly^6−$nGly^{10}$ (Leu^7O: −0.50 e)	cACE zinc-binding domain	7	−18.0 (3.7)	−11.8 (2.9)	5.2 (1.9)
A. Gly^6−$nGly^{10}$ (Leu^7O: −1.50 e)	cACE zinc-binding domain	12	−20.6 (3.6)	−15.0 (2.9)	5.0 (1.3)
B. $pGlu^1$−Tyr^5	cACE channel without Gly^6-Leu^7	12[b]	−15.9 (2.1)	−9.0 (1.9)	7.4 (1.4)
B. $pGlu^1$−Tyr^5	cACE channel with Gly^6-Leu^7	18	−16.9 (1.7)	−9.9 (1.5)	6.9 (1.2)

[a] (A) Docking of the C-terminal zinc-binding fragment by using the Kollman charge or by increasing the negative charge of the Leu^7 carbonyl oxygen atom. (B) Docking of the N-terminal fragment including or excluding the Gly^6−Leu^7 moiety of the top-ranked C-terminal fragment. The results are given per 100 docking rounds with the standard deviation in parenthesis; energies are in kcal·mol^{-1} and rmsd from the top-ranked solution in Å. [b] Nine of these are not meaningful because of steric hindrance at the zinc-bound docked conformations.

is used at the first phase of docking and is then regarded as part of the enzyme, which was found to introduce specificity in the orientation of the second ligand within a possible linker distance to the first ligand, while excluding any unproductive binding modes. In the case of ACE−GnRH complexes, the conformation selected for the subsequent MD runs was among the top-three ranked results and was within a calculated binding energy range of 1.5 kcal·mol^{-1}. The docking results obtained for each domain of ACE with GnRH in both orientations are summarized in Table 2 of the Supporting Information. Finally, the two GnRH fragments were linked together, and after the addition of the zinc-bound water molecule and the bonding of zinc with the scissile bond carbonyl oxygen, the substrate was subjected to energy minimization using the AMBER molecular mechanics force field.

Molecular Dynamics Calculations. Because the initial binding modes of GnRH were predicted by keeping the enzyme atoms in their crystallographic positions and in the absence of solvent molecules, we have employed molecular dynamics (MD) calculations as a means to introduce the effect of protein flexibility. Explicit solvent treatment was used so as to observe interactions between ACE and GnRH that are mediated by the polar solvent. In this way, it is possible to monitor local motions of the enzyme in the presence of the substrate at the nanosecond time scale and investigate the structural characteristics that govern their interaction. The scope of this study is to investigate the

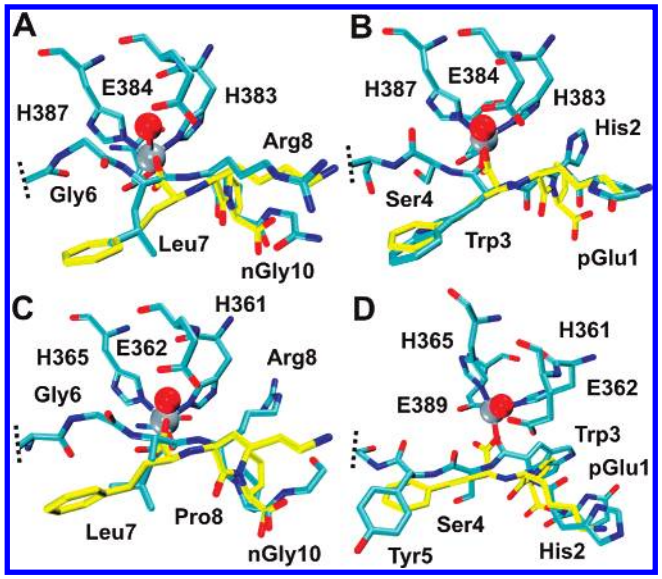

FIGURE 2: Initial conformations of the substrate's fragment P_2-P_1-P_1'-P_2' docked inside the two domains of ACE: (A) cACE−$GnRH_C$, (B) cACE−$GnRH_N$, (C) nACE−$GnRH_C$ and (D) nACE−$GnRH_N$. For comparison, the inhibitor lisinopril is shown at its crystallographic position as yellow sticks, zinc is shown as a gray sphere, and the zinc-bound water is in red.

enzyme−substrate interactions immediately prior to cleavage, either at the COOH- or at the NH_2-terminal tripeptides. For this reason, a water molecule is coordinated to Zn(II) so that it can attack the carbonyl carbon of the scissile bond. In order to accurately represent the zinc binding environment, force field parameters were extracted by carrying out DFT calculations on a model of the zinc-binding domain of ACE including *N*-methylacetamide as the substrate. This new set of AMBER force field parameters appears to be effective in representing the pentacoordinated zinc-binding geometry throughout MD calculations. The MD trajectories were analyzed in order to identify important intermolecular interactions by extracting their geometric features (distances and angles) as a function of simulation time. The major interactions between ACE and GnRH are summarized in Table 3. Hydrogen-bonding interactions were monitored using 3.5 Å as the distance cutoff and 120° as the angle cutoff, whereas hydrophobic interactions were included for a pair of carbon atoms at a distance shorter than 4.5 Å. Only interactions that are present more than half of the simulation time are considered, whereas water-mediated hydrogen bonds should be observed at least at 25% of the trajectory frames.

Overall Enzyme−Substrate Conformation. The four systems appear to be well equilibrated after the first 100 ps, as evident from the plots of the root-mean-square deviation (rmsd) of either Cα atoms of ACE or all atoms of GnRH from their initial coordinates and as a function of simulation time (Figure 3). For each enzyme−substrate complex, the average value and the standard deviation in Å were calculated for the total simulation time; cACE: 1.48 (0.23) − $GnRH_C$: 1.86 (0.18); cACE: 1.47 (0.25) − $GnRH_N$: 2.23 (0.28); nACE: 1.45 (0.19) − $GnRH_C$: 2.80 (0.48); nACE: 1.64 (0.24) − $GnRH_N$: 3.42 (0.45). Noticeably, the complex that exhibits the highest deviation from the initial coordinates is nACE with $GnRH_N$, in contrast to both complexes of cACE that display the lowest variations. However, this observation does not indicate that cACE complexes with GnRH are more stable, rather that the conformations of the substrate predicted by the docking calculations display less reorganization during the MD phase.

The radius of gyration (Rγ) of ACE in each complex with GnRH exhibits minute fluctuations during the course of the simulations (Figure 4A), thus supporting the stability of the overall compact structure of ACE. In remarkably good agreement with the initial value of $R\gamma = 23.62$ Å for cACE and $R\gamma = 24.45$ Å for nACE, the mean value calculated throughout the total simulation time with the standard deviation in parenthesis is 23.74 (0.06) for cACE−$GnRH_C$, 23.86 (0.05) for cACE−$GnRH_N$, 24.72 (0.08) for nACE−$GnRH_C$, and 24.69 (0.11) for nACE−$GnRH_N$. This is further supported by the plots of the accessible surface area of the enzyme complexes, which exhibit fluctuations within 2% of the initial value and are calculated to be 23404 (197) for cACE−$GnRH_C$, 23085 (254) for cACE−$GnRH_N$, 25730 (340) for nACE−$GnRH_C$, and 25847 (467) for nACE−$GnRH_N$ in Å^2 (Figure 4B). The buried surface area of GnRH as a function of simulation time is shown in Figure 4C and D and is calculated to be 1427 (25) for cACE−$GnRH_C$, 1431 (32) for cACE−$GnRH_N$, 1404 (37) for nACE−$GnRH_C$, and 1332 (25) for nACE−$GnRH_N$ in Å^2.

A hinge mechanism has been recently proposed for substrate entry into the active site cleft of tACE (*52*), on the basis of homology to human ACE2, which was crystallized both in an open conformation without inhibitor and in an inhibitor-bound closed conformation (pdb IDs: 1R4L and 1R42, respectively) (*53*). Normal-mode analysis revealed intrinsic flexibility about the active site of tACE so that six hinge regions could be identified: 98−125, 296−297, 400−409, 434−439, 535−537, and 569−578 (tACE numbering). In particular, region 98−125 lies close to the surface between the α2 lid helix and α4; region 569−578 lies between the conserved HEMGH motif and E411 that binds zinc so that hinging about this region results in opening up the catalytic site (*52*). The mobility of the simulated ACE−GnRH complexes was investigated by calculating the B-factors of the backbone Cα atoms from their root-mean square fluctuations during the 2-ns MD simulation (Figure 4). A comparison between the two domains of the enzyme with the orientations of the two substrates reveals that (i) region 98−125/71−98 (cACE/nACE) exhibits quite high *B*-factors, indicating that substrate binding into the catalytic cleft might not influence the mobility of residues about which the hinge opens; (ii) region 569−578 (cACE) exhibits low *B*-factors, whereas the corresponding 547−556 region in nACE shows some degree of flexibility that can be attributed to the loop region between helix α25 and α26; (iii) in both domains of ACE, the region between sheet β1 and the following loop up to sheet β2 exhibits high flexibility (i.e., residues 150−158 in cACE and 125−136 in nACE); (iv) in cACE, regions 292−299 (between helix α9 and α10) and 305−310 (before helix α11) display more than double the *B*-factors for $GnRH_C$ in comparison with those for $GnRH_N$, whereas the corresponding region in nACE (269−278) exhibits comparable high flexibility for both GnRH orientations; (v) in nACE, region 530−538 exhibits higher flexibility for $GnRH_N$ than for $GnRH_C$, in contrast to the corresponding region 552−560 in cACE that has equally low *B*-factors for both GnRH orientations; and (vi) the region between helix α14 and sheet β4 (320−327) in nACE appears to be more flexible in $GnRH_C$ than in $GnRH_N$.

Table 3: ACE Residues of Domains C and N that Exhibit Major Electrostatic Interactions with Both Orientations of GnRH[a]

ACE	S_7	S_6	S_5	S_4	S_3	S_2	S_1	S_1'	S_2'	S_3'	
C-domain	Lys118	Glu123	Glu403	Glu403	Asp358	Ala356	Ala354	Glu162	Lys511	Lys511	$GnRH_C$
	Trp59 **Thr92** **Val119** **Leu122**		Arg522 **Asp121** **Met223** **Phe570**	Glu411	**His410** **Trp357** **Tyr360** **Phe391**	*WAT*	Arg522 **His353** **Ser355** **Val518**	Asp377 His513 **Ala354** **Val380**	**Val380** **Phe457** **Phe519** **Tyr523**	His513	
	Lys118 Ser222 Tyr213	Glu123 Tyr51 **Tyr213**	Glu123 Glu403 **Trp59** **Ala400**	Glu403 **Trp220** **Ile204** **Pro519**	Arg522	Arg402 Tyr360 Arg522 **Trp357** **Phe391** **Glu403** **His410**	Pro519 *WAT*	**Trp357** **His513** **Phe512** **Val518**	Asp415 Asp453 His513 **Val379** **Val380** **Phe457** **Tyr523** **Phe527**	Glu162 His353 Glu376 **Ala354** **Val380** **Phe512**	$GnRH_N$
N-domain	Arg90	Gly382	Thr97	Tyr338	Asp336	Ala334	Ala332	His331	Gln259	−	$GnRH_C$
	Arg381 Ser548	Ala383 **Trp201** **Tyr338** **Pro385**	Arg500 **Leu32** **Thr97** **Leu98**	Tyr372 Gly382	Tyr372 Arg500 **Trp335** **Tyr338** **Tyr369**	Tyr369	Glu389 **His331** **Phe490** **His491**	Ser357 Thr358 Glu362 Asp393 His491	Lys489 **Phe435** **His491** **Tyr498** **Tyr501** **Phe505**		
	Ala94 Thr97	Arg381 **Leu32** **Tyr338**	Glu389 *CL2* **Tyr369** **His388**	Ala334 Tyr338 **Val36** **Trp335**	Ala334 *CL2*	Asp43 Lys364 Asn494 Arg500 **Val329** **Trp335** **Phe490**	His331 His491 *WAT*	Ala332 Asp393 **Phe435** **His491** **Tyr501** **Phe505**	Glu431 Asp393 **Phe505**	Ala332 Gln355 Thr358 **His331**	$GnRH_N$

[a] Residues that provide hydrophobic contacts are marked in bold, whereas those found to be water-mediated are underlined. The zinc-bound water is designated *WAT* and the buried chloride ion *CL2*.

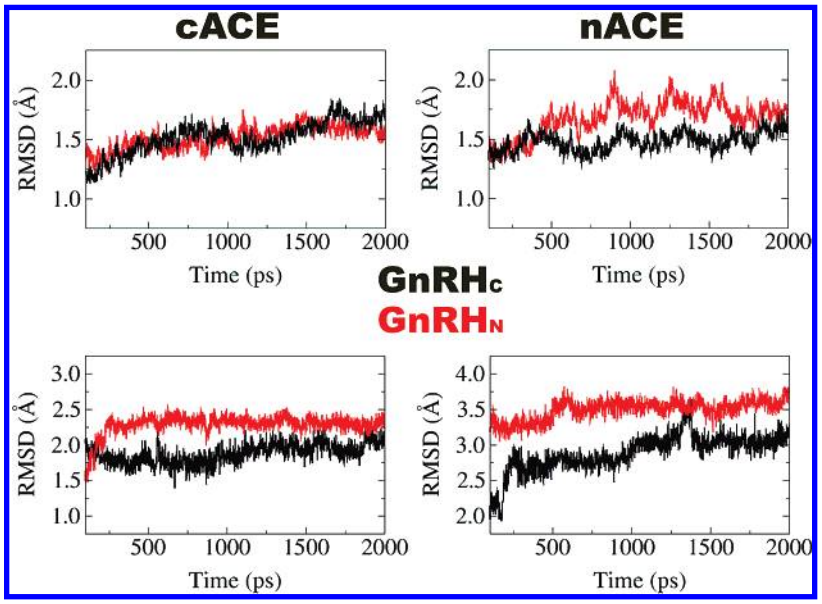

FIGURE 3: Root-mean-square deviation as a function of simulation time from the initial model of ACE Cα atoms (upper plots) and GnRH all atoms (lower plots) in the complex of cACE (left) or nACE (right) with $GnRH_C$ (black lines) or $GnRH_N$ (red lines).

Enzyme−Substrate Specific Interactions. By modeling of a Phe−His−Leu tripeptide substrate using the tACE−lisinopril structure, Sturrock et al. (*54*) have demonstrated that (i) Tyr523 promotes the formation of the intermediate similar to the role of His231 and Tyr157 in thermolysin by forming a hydrogen bond between the hydroxyl group and the scissile bond carbonyl oxygen; (ii) Ala354 plays a role similar to that of Ala113 in thermolysin by stabilizing the scissile bond nitrogen of the substrate via hydrogen-bonding interaction with its carbonyl oxygen. An examination of the calculated distances between the atoms of the GnRH scissile bond and either Tyr523/501 or Ala354/332 of cACE/nACE reveals that (i) the Tyr523/501 hydroxyl group is restricted at a distance of 3.5−4.5 Å from the scissile bond oxygen of both GnRH orientations and both ACE domains (Figure 5A in Supporting Information) and that (ii) although Ala354/332 is well positioned to interact with Arg^8NH in $GnRH_C$, this is not the case for Ser^4NH in $GnRH_N$, which is removed

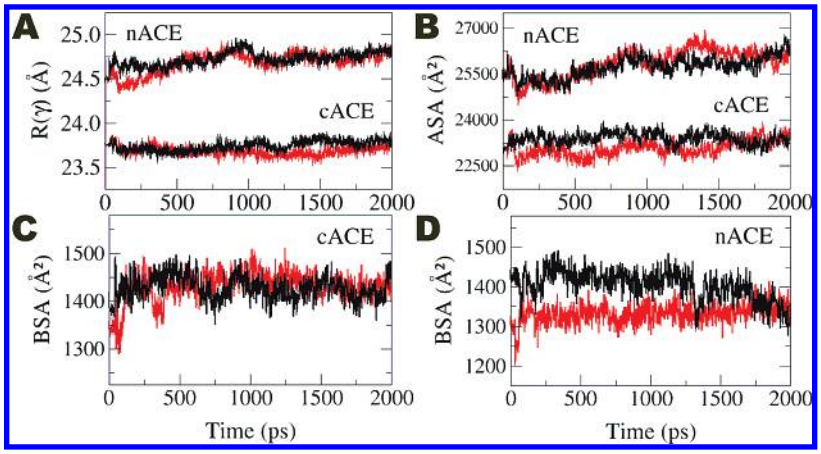

FIGURE 4: Time dependence of the radius of gyration, Rγ (A), accessible surface area of the enzyme, ASA (B), and buried surface area of the substrate, BSA (C, D) during the MD simulations of the ACE complexes with either $GnRH_C$ (black lines) or $GnRH_N$ (red lines).

from the carbonyl oxygen of either Ala354 in cACE or Ala332 in nACE (Figure 5B in Supporting Information). This observation implicates the placement of $GnRH_N$ scissile bond for primary amino-terminal endoproteolytic cleavage by ACE and raises the point whether a water-mediated interaction between Ala354/332 and Ser^4NH can compensate for a direct hydrogen bond.

Another interesting observation is that the carbonyl oxygen of either Ser^4 in $GnRH_N$ or Gly^6 in $GnRH_C$ forms a stable hydrogen bond with the zinc-bound water molecule of cACE. In contrast, the MD simulation of nACE reveals that only Ser^4O ($GnRH_N$) and not Gly^6O (GnRHc) is within proper hydrogen-bonding distance (Figure 6). Gly^6 of $GnRH_C$ exhibits a hydrogen bond with the Tyr369 hydroxyl group of nACE, a residue that is replaced by Phe391 in cACE. The latter exhibits van der Waals contacts with the neighboring Tyr^5 residue of $GnRH_C$ (Table 3). This observation implies that the carbonyl oxygen of the P_2-P_1 peptide bond (Ser^4O in $GnRH_N$ or Gly^6O in $GnRH_C$) might contribute to the enhancement of the zinc-bound water nucleophilicity via a hydrogen-bonding interaction, in conjunction with the polarization between zinc and Glu384/362 carboxylate that is proposed to promote water's attack on the carbon of the scissile bond (*14*). The absence of such an interaction in the nACE−$GnRH_C$ complex may be a factor that predisposes the endoproteolytic activity of nACE to NH_2-terminal substrate cleavage.

Interactions that Support $GnRH_C$ Cleavage by Both ACE Domains. By carrying out a series of sophisticated kinetic measurements on a variety of ACE substrates, Husain and co-workers have recently shed light on the basis of the exopeptidase activity of the C domain (*55*). This mainly involves the carboxylate-docking interactions with Lys511 and Tyr520, as was previously observed in the tACE-lisinopril crystal structure (*15*). Because GnRH is protected at both NH_2- and COOH-termini, such carboxylate-docking interactions become less important for transition-state stabilization. Analysis of our MD data reveals that the conserved Lys511/489 residue participates in the binding of $GnRH_C$ by forming a hydrogen bond with the Pro^9 backbone, in contrast to $GnRH_N$, where S_2' is occupied by the protonated His^2 and exhibits no interactions with Lys511/489. Concerning Tyr520/498, it appears to be involved only in the interaction of $GnRH_C$ with the S_2' subsite of nACE (Table 3). Therefore, cleavage of the C-terminal tripeptide of GnRH

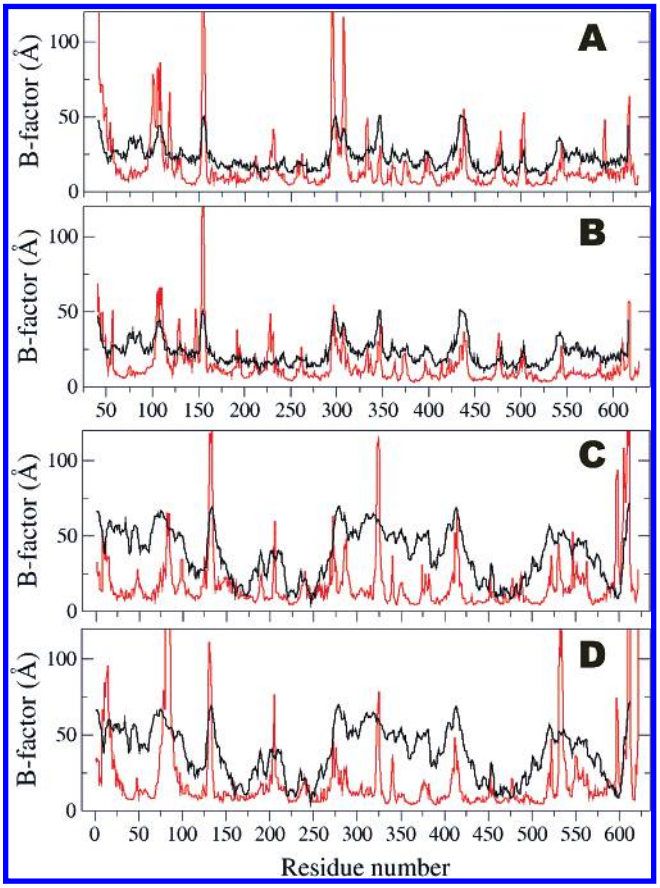

FIGURE 5: *B*-factors calculated from the atomic fluctuations of ACE Cα atoms during the course of the 2-ns MD trajectory (red) in comparison with the corresponding crystallographic values (black). (A) cACE−$GnRH_C$, (B) cACE−$GnRH_N$, (C) nACE−$GnRH_C$, and (D) nACE−$GnRH_N$ complexes.

is not expected to be strongly dependent on these two ACE residues that provide the carboxylate-docking interactions.

However, major electrostatic interactions are displayed at the S_1' that is occupied by Arg^8 of $GnRH_C$. In cACE, both Glu162 and Asp377 are predicted to form salt bridges with Arg^8, similar to Glu362 and Asp393 in nACE. Additional hydrogen-bonding interactions are provided by the conserved His513/491 residue of both ACE domains, in addition to Ser357 and Thr358 of nACE (Table 3). These interactions are thus expected to contribute significantly to the endoproteolytic cleavage of the GnRH C-terminus by both domains

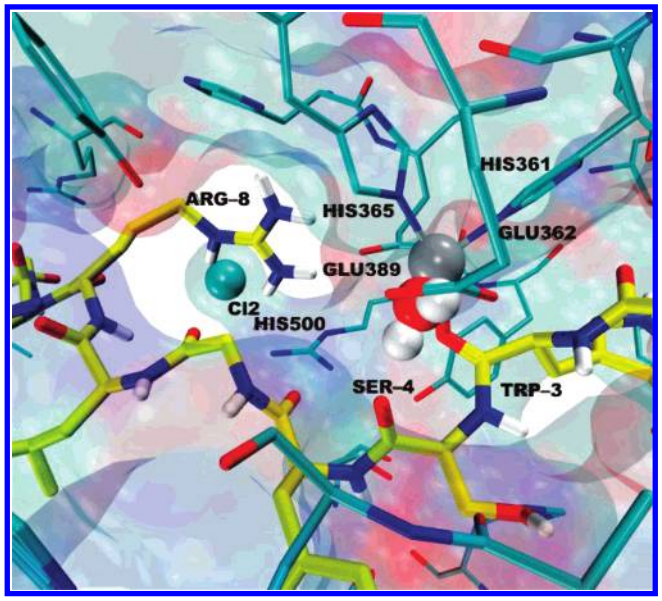

FIGURE 6: Representation of the chloride binding site of the nACE (cyan sticks)−$GnRH_N$ (yellow sticks) complex. The Cl2 ion is shown as a green sphere, the zinc ion is in gray, and the zinc-bound water is in red.

of ACE. Furthermore, the S_2' subsite in both ACE domains accommodates Pro^9 of $GnRH_C$ into a hydrophobic cage of aromatic rings comprising Phe and Tyr residues (Figure 7B and D). This is also the case for Leu^7, which is well positioned to exhibit both hydrophobic and hydrogen-bonding interactions at the S_1 subsite of ACE.

Apart from the interactions observed near the zinc-binding site, the S_3−S_7 subsites provide major interactions with $GnRH_C$. The P_5 residue Trp^3 of $GnRH_C$ interacts with the chloride-binding Arg522/500 residue of cACE/nACE and exhibits hydrophobic interactions with Phe570 and Met223 of cACE or Leu32 and Leu98 of nACE. Interestingly, the S_3 subsite provides major interaction with Tyr^5 of $GnRH_C$ in contrast to $GnRH_N$ where Gly^6 exhibits fewer interactions with either domain of ACE. The conserved Asp358/336 residue backbone forms stable hydrogen bonds with Tyr^5, whereas Tyr372 of nACE provides further stabilization with $GnRH_C$ (Table 3). The conserved Trp357/335 of ACE and Phe391 of cACE or the corresponding Tyr369 of nACE exhibit van der Waals contacts with the Tyr^5 side chain. Finally, the S_7 subsite with Lys118 in cACE or Arg90 and Arg381 in nACE provide the appropriate context for interaction with the polar groups of $pGlu^1$ in $GnRH_C$. In addition, a hydrophobic cage comprising Trp59, Val119, and Leu122 accommodates $pGlu^1$ in cACE, interactions that were not detected in the simulations of nACE−$GnRH_C$. However, $pGlu^1$ along with Trp^3 and Tyr^5 of GnRH orientation for COOH-terminal cleavage displays similar interactions with both domains of ACE.

Interactions that Support $GnRH_N$ Cleavage by nACE. Remarkably, in all MD trajectories, the conserved Arg522/500 residue of cACE/nACE exhibits either direct or water-mediated hydrogen-bonding interactions with GnRH (Table 3). This residue is one of the three Cl2 ligands (Tyr224/202 and a water molecule are the other two) and is reported to be critical for the chloride dependence of ACE activity (*56*). Our results indicate that there is a direct interaction between both Arg522 and Arg500 and Tyr^5 of $GnRH_N$, whereas for $GnRH_C$, Trp^3 exhibits water-mediated hydrogen bonds with Arg522 in cACE or Arg500 in nACE. This finding is in agreement with a previous suggestion that this residue, which lies on the same helix (α17 of tACE) as that of two residues (Tyr520 and Tyr523) that interact with the inhibitor, may interact with the substrate as well (*15*).

What is of more interest is that only in the simulation of the nACE−$GnRH_N$ complex does the guanidine group of Arg^8 display a strong electrostatic interaction with the Cl2 ion, a contact that is not present in the initial docked conformation. This interaction results in an nACE $Arg500^{+}\cdots Cl^{-}\cdots{}^{+}Arg^8$ substrate bridge, which can increase the stability of the ground and transition states (Figure 6). In addition to this, Arg^8 is found to stabilize the zinc-binding Glu389 through a hydrogen bond between the guanidine and carboxylate (Figure 6 in Supporting Information), an interaction that might further increase the affinity of the enzyme−substrate complex. At this point, it must be noted that Tyr202 (the other Cl2 ligand in nACE) is displaced upon the interaction of Arg^8 with the chloride ion.

On the basis of an earlier report that the affinity of chloride binding to ACE is increased with substrates that contain a basic P_2' side chain, particularly that of arginine (*19*), an analogous bridging interaction has been recently proposed for cACE and P_2' Arg (*55*). From our data, the protonated His^2 (P_2') residue of $GnRH_N$ does not appear to be implicated in such an interaction; however, this hypothesis seems to be plausible on a structural basis for a basic residue in a position other than the P_2', for example, Arg^8 of $GnRH_N$. Taking into account that in all the other MD simulations of GnRH with ACE (Table 3) there is no direct interaction with Cl2, this ionic bridge might play a major role in the endoproteolytic cleavage of GnRH by nACE, which is in agreement with experimental evidence that the N domain of ACE is mainly responsible for the primary NH_2-terminal cleavage of GnRH (*24*, *28*).

Recently, Sturrock and co-workers synthesized a lisinopril−tryptophan analogue inhibitor of ACE (*57*) on the basis of the interactions of the phosphonic acid inhibitor RXPA380 (*23*). Molecular modeling studies have revealed that the indole−NH has the ability to establish a strong hydrogen bond with Asp453 of cACE and that the tryptophan makes hydrophobic interactions with Val379 and Val380. This is also apparent for Trp^3 of $GnRH_N$, which displays hydrogen-bonding interactions with Asp393 at the S_1' of nACE (Table 3), in contrast to cACE for which such an interaction is not observed (Figure 7B and D). Therefore, the P_1' residue of $GnRH_N$ is predicted to contribute appreciably to the specificity of nACE for NH_2-terminal cleavage.

Interactions that Contribute to the Affinity of the ACE−GnRH Complex. A number of important interactions between ACE and GnRH cannot be strictly classified as described above but are predicted to contribute significantly to the *in vitro* endoproteolytic activity of ACE. The P_2' basic histidine residue of $GnRH_N$ exhibits strong electrostatic interactions with both domains of ACE, if it is protonated. Specifically, Asp415 and Asp453 residues of cACE or Asp393 and Glu431 of nACE form hydrogen bonds with the His^2 imidazole ring. The conserved Phe527/505 residue exhibits van der Waals contacts with His^2 of $GnRH_N$ in both ACE domains, whereas Val379 and Val380 of cACE that exhibit contacts with $GnRH_N$ are replaced by the polar Ser357 and

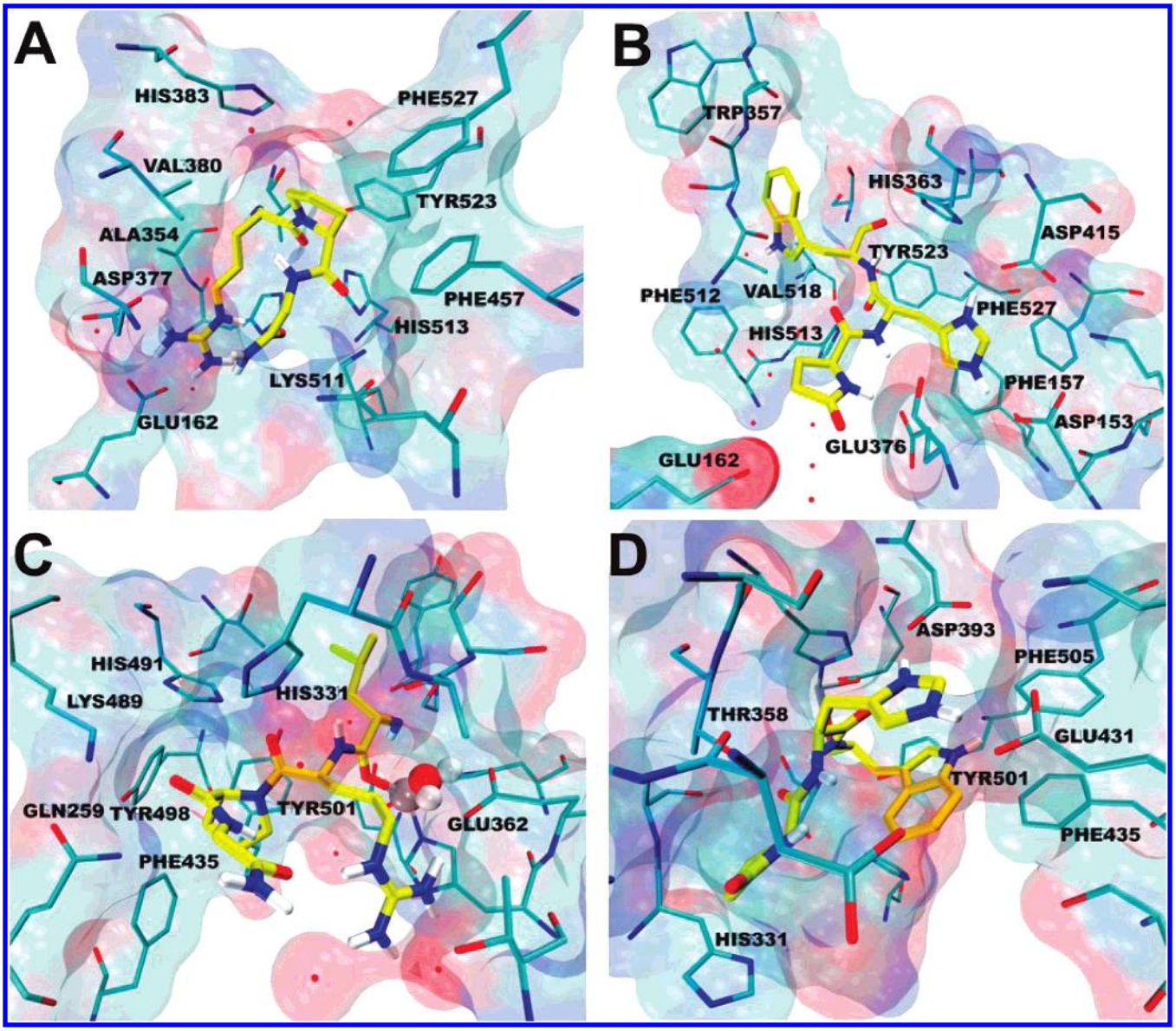

FIGURE 7: S prime subsites of (A) cACE−$GnRH_C$, (B) cACE−$GnRH_N$, (C) nACE−$GnRH_C$, and (D) nACE−$GnRH_N$ complexes; representations are as in Figure 6.

Thr358 residues in the S_1' subsite of nACE. As far as the S_3' subsite is concerned, $pGlu^1$ of $GnRH_N$ exhibits electrostatic and hydrophobic interactions with both domains of ACE, though cACE is predicted to provide more interactions directly (Table 3). On the basis of these observations, it is predicted that P_2' and P_3' residues might contribute equally to the affinity of both ACE domains for $GnRH_N$.

Even though Gly^6 exhibits a few contacts in both GnRH orientations, this residue is predicted to mediate some key interactions. Particularly for $GnRH_C$, Gly^6 provides additional stabilization to the zinc-bound water of cACE, whereas for nACE, it is implicated in two hydrogen bonds with Ala334 and Tyr369 (Table 3). At the opposite orientation, Gly^6 of $GnRH_N$ is predicted to interact with the chloride-binding site, either directly with Arg522 of cACE or by a water-mediated interaction with the Cl2 ion of nACE. As far as the S_4 subsite is concerned, Glu403 of cACE exhibits interactions with either the Ser^4 hydroxyl group of $GnRH_C$ or the Leu^7 backbone of $GnRH_N$, whereas in nACE, this residue is replace by Tyr338. In addition, Leu^7 of $GnRH_N$ makes hydrophobic contacts with Trp220 and Ile204 of cACE or Val36 and Trp335 of nACE (Table 3).

As discussed above, Arg^8, which occupies the S_5 subsite of the nACE−$GnRH_N$ complex, is able to bind the Cl2 ion. In cACE, Arg^8 is predicted to be implicated in a salt bridge with Glu123, a residue that can also provide electrostatic interactions with His^2 of $GnRH_C$ or the Pro^9 carboxylate group of $GnRH_N$ at the S_6 subsite of cACE (Table 3). In nACE, this residue is replaced by Gly99, which cannot mediate similar interactions; however, Gly382 and Ala383 display hydrogen bonds with His^2 of $GnRH_C$ and Arg381 with Pro^9 of $GnRH_N$. Further stabilization through hydrophobic contacts with His^2 is provided by Trp201 and Tyr338 of nACE, in contrast to cACE for which no such interactions were observed. Pro^9 makes van der Waals contacts with Tyr213 of cACE or Leu32 and Tyr338 of nACE (Table 3).

As far as the protected termini of GnRH are concerned, $nGly^{10}$ of $GnRH_N$ displays hydrogen-bonding interactions with Lys118, Ser222, and Tyr213 at the S_7 of cACE, or Ala94 and Thr97 of nACE. In the opposite orientation, $nGly^{10}$

on $GnRH_C$ reveals minor interactions with both ACE domains at the S_3' subsites, which are mainly water-mediated hydrogen bonds. In contrast, when the S_3' subsite is occupied by $pGlu^1$ of $GnRH_N$, major interactions are exhibited with both ACE domains and especially with cACE (Table 3). This residue was also predicted to exhibit strong electrostatic and hydrophobic interactions at the S_7 subsite of the cACE−$GnRH_C$ complex.

CONCLUSIONS

Although the precise biological role of ACE in the processing of GnRH is unclear, there are several studies that suggest that it might be important for the degradation of the hormone. Alternative peptidases are capable of hydrolyzing the C-terminal residues from prohormone intermediates in mice lacking carboxypeptidase activity (*58*). Among these, somatic ACE efficiently removes the C-terminal dipeptide from the Gly-Lys-Arg-extended GnRH. Furthermore, enzymatic degradation of GnRH by intestinal mucosal tissues is regulated by endopeptidase-24.18 (EC 3.4.24.18), endopeptidase-24.15 (EC 3.4.24.15), and ACE as indicated by the formation of $GnRH_{(1-3)}$ and $GnRH_{(1-4)}$ (*59*). Finally, the activity of GnRH-inactivating peptidases may vary in different reproductive states such as across the estrous cycle, and recently, Shimizu et al. showed the altered expression of ACE mRNA during the periovulatory phase in GnRH-treated cows (*60*). Thus, the elucidation of the mechanism of how ACE cleaves this important hormone is key to our understanding of ACE's possible role in the endocrine system.

A series of docking calculations in combination with MD simulations have been carried out in order to study the structural characteristics of an ACE−GnRH complex. The substrate was docked inside the catalytic groove of both domains of ACE in appropriate conformation for either COOH- or NH_2-terminal endoproteolytic cleavage, and the reorganization of their complex was monitored by MD calculations. Although both domains of ACE provide the appropriate context for either direct or water-mediated interactions with the substrate, our data indicate that the N domain of ACE provides an additional electrostatic interaction with the substrate, which may explain its preference for the primary amino-terminal endoproteolytic cleavage of GnRH *in vitro*. On a structural basis, it is possible that the Arg^8 guanidine side chain of $GnRH_N$ interacts directly with the chloride ion of nACE as well as stabilizes the zinc-bound Glu389 carboxylate through hydrogen-bonding interaction. Such an interface is predicted to comprise an nACE $Arg500^+\cdots Cl^-\cdots {}^+Arg^8$ $GnRH_N$ bridging interaction. In support of this observation, the protected N-terminal $pGlu^1$ residue of $GnRH_N$ exhibits stronger interactions in the S_3' subsite of both ACE domains, with respect to those provided by the amidated C-terminal $nGly^{10}$ of $GnRH_C$. By virtue of the absence of any C-terminal carboxylate-docking interactions with the protected peptide, the contribution of $pGlu^1$ in stabilizing the ground and transition states of the enzyme−substrate complex may play a key role.

Moreover, apart from the carboxylate group of Glu384/362 in cACE/nACE that polarizes the zinc-bound water that attacks the carbon of the scissile bond, Ser^4 or the Gly^6 carbonyl oxygen of $GnRH_N$ or $GnRH_C$, respectively, exhibits additional stabilization through a hydrogen bond with the zinc-bound water. This has been observed in all MD simulations with the exception of that of the nACE−$GnRH_C$ complex. However, both orientations of GnRH display hydrogen-bonding interactions with the conserved Arg522/500 chloride-binding residue, either directly or in a water-mediated manner, interactions that support the basis of the chloride-dependent activity of ACE.

In conclusion, this simulation study of a zinc−metalloprotease complex with a peptide substrate reveals valuable information on the structural determinants of their interaction and offers new insights into the dynamic nature of their binding. The data reported here provide a structural basis for the chloride-dependent activity of ACE and an appreciation of new enzyme−substrate contacts that contribute to substrate recognition. In addition, these simulations provide an extended view of the catalytic subsites that are more distant from the metal center in comparison with those identified by the small-molecule inhibitors. These findings are likely to contribute to the targeting of the distal binding subsites in the design of next-generation domain-selective inhibitors of ACE with improved pharmacological profiles.

ACKNOWLEDGMENT

We thank the referees for their constructive comments on the manuscript. A.P. is grateful to Yannis Lazarou for his assistance with the Gaussian calculations and to David Case for providing the AMBER software.

NOTE ADDED AFTER ASAP PUBLICATION

This article was released ASAP on July 3, 2007, with a minor error in one of the pdb codes in the first paragraph of the Computational Methods section. The correct version was posted on July 13, 2007.

SUPPORTING INFORMATION AVAILABLE

A figure with the model of the catalytic site of ACE used for the DFT calculations, a table with important geometrical features of the zinc coordination sphere and the derived AMBER force field parameters, four figures with plots of selected distances and angles versus simulation time of ACE with GnRH, a table summarizing the docking results of each GnRH fragment with both ACE domains, and a figure illustrating the highest docked conformations of the cACE−$GnRH_C$ complex. This material is available free of charge via the Internet at http://pubs.acs.org.

REFERENCES

1. Kearney, P. M., Whelton, M., Reynolds, K., Muntner, P., Whelton, P. K., and He, J. (2005) Global burden of hypertension: analysis of worldwide data, *Lancet 365*, 217−223.
2. Inagami, T. (1994) The renin-angiotensin system, *Essays Biochem. 28*, 147−164.
3. Turner, A. J., and Hooper, N. M. (2002) The angiotensin-converting enzyme gene family: genomics and pharmacology, *Trends Pharmacol. Sci. 23*, 177−183.
4. Patchett, A. A., Harris, E., Tristram, E. W., Wyvratt, M. J., Wu, M. T., Taub, D., Peterson, E. R., Ikeler, T. J., ten Broeke, J., Payne, L. G., Ondeyka, D. L., Thorsett, E. D., Greenlee, W. J., Lohr, N. S., Hoffsommer, R. D., Joshua, H., Ruyle, W. V., Rothrock, J. W., Aster, S. D., Maycock, A. L., Robinson, F. M., Hirschmann, R., Sweet, C. S., Ulm, E. H., Gross, D. M., Vassil, T. C., and Stone, C. A. (1980) A new class of angiotensin-converting enzyme inhibitors, *Nature 288*, 280−283.

5. Zaman, M. A., Oparil, S., and Calhoun, D. A. (2002) Drugs targeting the renin-angiotensin-aldosterone system, *Nat. Rev. Drug Discovery 1*, 621−636.
6. Acharya, K. R., Sturrock, E. D., Riordan, J. F., and Ehlers, M. R. (2003) ACE revisited: a new target for structure-based drug design, *Nat. Rev. Drug Discovery 2*, 891−969.
7. Turk, B. (2006) Targeting proteases: successes, failures and future prospects, *Nat. Rev. Drug Discovery 5*, 785−799.
8. Barrett, A. J. (1998) Introduction: other Families in Clan MA, in *Handbook of Proteolytic Enzymes* (Barret, A. J., Rawlings, N. D., and Woessner, J. F., Eds.), pp 1033−1037, Academic Press, New York.
9. Corvol, P., Williams, T. A., and Soubrier, F. (1995) Peptidyl dipeptidase A: angiotensin I-converting enzyme, *Methods Enzymol. 248*, 283−305.
10. Hubert, C., Houot, A. M., Corvol, P., and Soubrier, F. (1991) Structure of the angiotensin I-converting enzyme gene. Two alternate promoters correspond to evolutionary steps of a duplicated gene, *J. Biol. Chem. 266*, 15377−15383.
11. Ehlers, M. R., Fox, E. A., Strydom, D. J., and Riordan, J. F. (1989) Molecular cloning of human testicular angiotensin-converting enzyme; the testis isoenzyme is identical to the C-terminal half of endothelial angiotensin-converting enzyme, *Proc. Natl. Acad. Sci. U.S.A. 86*, 7741−7745.
12. Soubrier, F., Alhenc-Gelas, F., Hubert, C., Allegrini, J., John, M., Tregear, G., and Corvol, P. (1988) Two putative active centers in human angiotensin I-converting enzyme revealed by molecular cloning, *Proc. Natl. Acad. Sci. U.S.A. 85*, 9386−9390.
13. Matthews, B. W. (1988) Structural basis of the action of thermolysin and related zinc peptidases, *Acc. Chem. Res. 21*, 333−340.
14. Hangauer, D. G., Monzinqo, A. F., and Matthews, B. W. (1984) An interactive computer graphics study of thermolysin-catalyzed peptide cleavage and inhibition by N-carboxymethyl dipeptides, *Biochemistry 23*, 5730−5741.
15. Natesh, R., Schwager, S. L. U., Sturrock, E. D., and Acharya, K. R. (2003) Crystal structure of the human angiotensin-converting enzyme-lisinopril complex, *Nature 421*, 551−554.
16. Corradi, H. R., Schwager, S. L. U., Nchinda, A. T., Sturrock, E. D., and Acharya, K. R. (2006) Crystal structure of the N domain of human somatic angiotensin I-converting enzyme provides a structural basis for domain-specific inhibitor design, *J. Mol. Biol. 357*, 964−974.
17. Redelinghuys, P., Nchinda, A. T., and Sturrock, E. D. (2005) Development of domain-selective angiotensin I-converting enzyme inhibitors, *Ann. N.Y. Acad. Sci. 1056*, 160−175.
18. Spyroulias, G. A., and Cordopatis, P. (2005) Current inhibition concepts of zinc metallopeptidases involved in blood pressure regulation, *Curr. Enz. Inhibition 1*, 29−42.
19. Shapiro, R., Holmquist, B., and Riordan, J. F. (1983) Anion activation of angiotensin converting enzyme: dependence on nature of substrate, *Biochemistry 22*, 3850−3857.
20. Natesh, R., Schwager, S. L. U., Evans, H. R., Sturrock, E. D., and Acharya, K. R. (2004) Structural details on the binding of antihypertensive drugs captopril and enalaprilat to human testicular angiotensin I-converting enzyme, *Biochemistry 43*, 8718−8724.
21. Wei, L., Clausen, E., Alhenc-Gelas, F., and Corvol, P. (1992) The two homologous domains of angiotensin I-converting enzyme interact differently with competitive inhibitors, *J. Biol. Chem. 267*, 13398−13405.
22. Dive, V., Cotton, J., Yiotakis, A., Michaud, A., Vassiliou, S., Jiracek, J., Vazeux, G., Chauvet, M. T., Cuniasse, P., and Corvol, P. (1999) RXP407, a phosphonic peptide, is a potent inhibitor of angiotensin I converting enzyme able to differentiate between its two active sites, *Proc. Natl. Acad. Sci. U.S.A. 96*, 4330−4335.
23. Georgiadis, D., Cuniasse, P., Cotton, J., Yiotakis, A., and Dive, V. (2004) Structural determinants of RXPA380, a potent and highly selective inhibitor of the angiotensin-converting enzyme C-domain, *Biochemistry 43*, 8048−8054.
24. Jaspard, E., Wei, L., and Alhenc-Gelas, F. (1993) Differences in the properties and enzymatic specificities of the two active sites of angiotensin-I converting enzyme (kininase II). Studies with bradykinin and other natural peptides, *J. Biol. Chem. 268*, 9496−9503.
25. Deddish, P. A., Marcic, B., Jackman, H. L., Wang, H. Z., Skidgel, R. A., and Erdos, E. G. (1998) N-domain-specific substrate and C-domain inhibitors of angiotensin-converting enzyme: angiotensin-(1−7) and keto-ACE, *Hypertension 31*, 912−917.
26. Rousseau, A., Michaud, A., Chauvet, M. T., Lenfant, M., and Corvol, P. (1995) The hemoregulatory peptide N-Acetyl-Ser-Asp-Lys-Pro is a natural and specific substrate of the N-terminal active site of human angiotensin-converting enzyme, *J. Biol. Chem. 270*, 3656−3661.
27. Skidgel, R. A., and Erdos, E. G. (1985) Novel activity of human angiotensin I converting enzyme: release of the NH2- and COOH-terminal tripeptides from the luteinizing hormone-releasing hormone. *Proc. Natl. Acad. Sci. U.S.A. 82*, 1025−1029.
28. Ehlers, M. R., and Riordan, J. F. (1991) Angiotensin-converting enzyme: zinc- and inhibitor-binding stoichiometries of the somatic and testis isoenzymes, *Biochemistry 30*, 7118−7126.
29. Case, D. A., Darden, T. A., Cheatham III, T. E., Simmerling, C. L., Wang, J., Duke, R. E., Luo, R., Merz, K. M., Jr., Wang, B., Pearlman, D. A., Crowley, M., Brozell, S., Tsui, V., Gohlke, H., Mongan, J., Hornak, V., Cui, G., Beroza, P., Schafmeister, C., Caldwell, J. W., Ross, W. S., and Kollman P. A. (2004) *AMBER 8*, University of California, San Francisco, CA.
30. Bashford, D., and Karplus, M. (1990) pKa of ionizable groups in proteins: atomic detail from a continuum electrostatic model, *Biochemistry 29*, 10219−10225.
31. Tsui, V., and Case, D. A. (2001) Theory and applications of the generalized Born solvation model in macromolecular simulations, *Biopolymers 56*, 275−291.
32. Wang, J., Wolf, R. M., Caldwell, J. W., Kollman, P. A., and Case, D. A. (2004) Development and testing of a general Amber force field, *J. Comput. Chem. 25*, 1157−1174.
33. Jakalian, A., Jack, D. B., and Bayly, C. I. (2002) Fast, efficient generation of high-quality atomic charges. AM1-BCC model: II. Parameterization and validation, *J. Comput. Chem. 23*, 1623−1641.
34. Morris, G. M., Goodsell, D. S., Halliday, R. S., Huey, R., Hart, W. E., Belew, R. K., and Olson, A. J. (1998) Automated docking using a Lamarckian genetic algorithm and an empirical binding free energy function, *J. Comput. Chem. 19*, 1639−1662.
35. Cornell, W. D., Cieplak, P., Bayly, C. I., Gould, I. R., Merz, K. M., Jr., Ferguson, D. M., Spellmeyer, D. C., Fox, T., Caldwell, J. W., and Kollman, P. A. (1995) A second generation force field for the simulation of proteins, nucleic acids, and organic molecules, *J. Am. Chem. Soc. 117*, 5179−5197.
36. Jorgensen, W. L., Chandrasekhar, J., Madura, J., and Klein, M. L. (1983) Comparison of simple potential functions for simulating liquid water, *J. Chem. Phys. 79*, 926−935.
37. Miyamoto, S., and Kollman, P. A. (1992) Settle: an analytical version of the SHAKE and RATTLE algorithm for rigid water models, *J. Comput. Chem. 13*, 952−962.
38. Berendsen, H. J. C., Postma, J. P. M., van Gunsteren, W. F., DiNola, A., and Haak, J. R. (1984) Molecular dynamics with coupling to an external bath, *J. Chem. Phys. 81*, 3684−3690.
39. Humphrey, W., Dalke, A., and Schulten, K. (1996) VMD: visual molecular dynamics, *J. Mol. Graphics 14*, 33−38.
40. Sanner, M. F., Spehner, J.-C., and Olson, A. J. (1996) Reduced surface: an efficient way to compute molecular surfaces, *Biopolymers 38*, 305−320.
41. Stote, R. H., and Karplus, M. (1995) Zinc binding in proteins and solution: a simple but accurate nonbonded representation, *Proteins 23*, 12−31.
42. Donini, O. A. T., and Kollman, P. A. (2000) Calculation and prediction of binding free energies for the matrix metalloproteinases, *J. Med. Chem. 43*, 4180−4188.
43. Merz, K. M., Jr. (1991) C02 Binding to human carbonic anhydrase II, *J. Am. Chem. Soc. 113*, 406−411.
44. Frisch, M. J., Trucks, G. W., Schlegel, H. B., Scuseria, G. E., Robb, M. A., Cheeseman, J. R., Zakrzewski, V. G., Montgomery, J. A., Jr., Stratmann, R. E., Burant, J. C., Dapprich, S., Millam, J. M., Daniels, A. D., Kudin, K. N., Strain, M. C., Farkas, O., Tomasi, J., Barone, V., Cossi, M., Cammi, R., Mennucci, B., Pomelli, C., Adamo, C., Clifford, S., Ochterski, J., Petersson, G. A., Ayala, P. Y., Cui, Q., Morokuma, K., Malick, D. K., Rabuck, A. D., Raghavachari, K., Foresman, J. B., Cioslowski, J., Ortiz, J. V., Stefanov, B. B., Liu, G., Liashenko, A., Piskorz, P., Komaromi, I., Gomperts, R., Martin, R. L., Fox, D. J., Keith, T., Al-Laham, M. A., Peng, C. Y., Nanayakkara, A., Gonzalez, C., Challacombe, M., Gill, P. M. W., Johnson, B. G., Chen, W., Wong, M. W., Andres, J. L., Head-Gordon, M., Replogle, E. S., Pople, J. A. (1998) *Gaussian 98*, revision A.9, Gaussian, Inc., Pittsburgh, PA.

45. Pelmenschikov, V., Blomberg, M. R. A., and Siegbahn, P. E. M. (2002) A theoretical study of the mechanism for peptide hydrolysis by thermolysin, *J. Biol. Inorg. Chem. 7*, 284−298.
46. Hoops, S. C., Anderson, K. W., and Merz, K. M., Jr. (1991) Force field design for metalloproteins, *J. Am. Chem. Soc. 113*, 8262−8270.
47. Tuccinardi, T., Martinelli, A., Nuti, E., Carelli, P., Balzano, F., Uccello-Barretta, G., Murphy G., and Rossello, A. (2006) Amber force field implementation, molecular modelling study, synthesis and MMP-1/MMP-2 inhibition profile of (R)- and (S)-N-hydroxy-2-(N-isopropoxybiphenyl-4-ylsulfonamido)-3-methylbutanamides, *Bioorg. Med. Chem. 14*, 4260−4276.
48. Park, H., and Merz, K. M., Jr. (2005) Force field design and molecular dynamics simulations of the carbapenem- and cephamycin-resistant dinuclear zinc metallo-*β*-lactamase from *Bacteroides fragilis* and its complex with a biphenyl tetrazole inhibitor, *J. Med. Chem. 48*, 1630−1637.
49. Park, H., and Lee, S. (2004) Homology modeling, force field design, and free energy simulation studies to optimize the activities of histone deacetylase inhibitors, *J. Comput.-Aided Mol. Des. 18*, 375−388.
50. Bayly, C. I., Cieplak, P., Cornell, W. D., and Kollman, P. A. (1993) A well-behaved electrostatic potential based method using charge restraints for deriving atomic charges: the RESP model, *J. Phys. Chem. 97*, 10269−10280.
51. Lin, J.-H., Perryman, A. L., Schames, J. R., and McCammon, A. J. (2002) Computational drug design accommodating receptor flexibility: the relaxed complex scheme, *J. Am. Chem. Soc. 124*, 5632−5633.
52. Watermeyer, J. M., Sewell, B. T., Schwager, S. L., Natesh, R., Corradi, H. R., Acharya, K. R., and Sturrock, E. D. (2006) Structure of testis ACE glycosylation mutants and evidence for conserved domain movement, *Biochemistry 45*, 12654−12663.
53. Towler, P., Staker, B., Prasad, S. G., Menon, S., Tang, J., Parsons, T., Ryan, D., Fisher, M., Williams, D., Dales, N. A., Patane, M. A., and Pantoliano, M. W. (2004) ACE2 X-ray structures reveal a large hinge-bending motion important for inhibitor binding and catalysis, *J. Biol. Chem. 279*, 17996−18007.
54. Sturrock, E. D., Natesh, R., van Rooney, J. M., and Acharya, K. R. (2004) Structure of angiotensin I-converting enzyme, *Cell. Mol. Life Sci. 61*, 2677−2686.
55. Naqvi, N., Liu, K., Graham, R. M., and Husain, A. (2005) Molecular basis of exopeptidase activity in the C-terminal domain of human angiotensin I-converting enzyme: insights into the origins of its exopeptidase activity, *J. Biol. Chem. 280*, 6669−6675.
56. Liu, X., Fernandez, M., Wouters, M. A., Heyberger, S., and Husain, A. (2001) Arg(1098) is critical for the chloride dependence of human angiotensin I-converting enzyme C-domain catalytic activity, *J. Biol. Chem. 276*, 33518−33525.
57. Nchinda, A. T., Chibale, K., Redelinghuys, P., and Sturrock, E. D. (2006) Synthesis and molecular modeling of a lisinopril-tryptophan analogue inhibitor of angiotensin I-converting enzyme, *Bioorg. Med. Chem. Lett. 16*, 4616−4619.
58. Isaac, R. E., Michaud. A., Keen, J. N., Williams, T. A., Coate, S. D., Wetsel, W. C., and Corvol, P. (1999) Hydrolysis by somatic angiotensin-I converting enzyme of basic dipeptides from a cholecystokinin/gastrin and a LH-RH peptide extended at the C-terminus with gly-Arg/Lys-arg, but not from diarginyl insulin, *Eur. J. Biochem. 262*, 569−574.
59. Wen, J. Y., Ledger, R., McLeod, B. J., Davies, N. M., Butt, A. G., and Tucker, I. G. (2002) Enzymatic degradation of luteinizing hormone releasing hormone (LHRH) by mucosal homogenates from the intestine of the common brushtail possum (*Trichosurus vulpecula*), *Life Sci. 71*, 3019−3030.
60. Shimizu, T., Berisha, B., Schams, D., and Miyamoto, A. (2007) Changes in the Messenger RNA expressions of the endothelin-1 and angiotensin systems in mature follicles of the superovulated bovine ovary, *J. Reprod. Dev.*, in press.

BI700253Q